

# Output Saturation and Linearity of Waveguide Unitraveling-Carrier Photodiodes

Jonathan Klamkin, *Student Member, IEEE*, Yu-Chia Chang, Anand Ramaswamy, *Student Member, IEEE*, Leif A. Johansson, *Member, IEEE*, John E. Bowers, *Fellow, IEEE*, Steven P. DenBaars, *Fellow, IEEE*, and Larry A. Coldren, *Fellow, IEEE*

**Abstract**—Waveguide unitraveling-carrier photodiodes (UTC-PDs) with different absorber and collector layer doping levels have been fabricated and characterized. These photodiode (PD) structures are fabricated on a platform that allows for the monolithic integration of multiquantum-well optical phase modulators and couplers for realizing novel coherent receivers. Compared to PD A, PD B has a lower and more graded p-doping profile in the absorber layer and also a higher n-doping level in the collector layer. For PD B a larger field is induced in the absorber layer at high photocurrent levels. Also the higher n-doping in the collector layer is adequate for providing charge compensation. For PD B, there is an enhancement in the RF response as the photocurrent level is increased. At a frequency of 1 GHz, the saturation current for PD A is around 65 mA and that for PD B is around 63 mA. For PD B, the third-order output intercept point at photocurrent levels of 30 and 40 mA is 37.2 and 34.9 dBm, respectively. That for PD A is 35.8 and 30.4 dBm. PD B is, therefore, favorable for linear operation at high current levels.

**Index Terms**—Coherent receiver, fiber-optic link, linearity, saturation current, third-order intermodulation distortion (IMD3), third-order output intercept point (OIP3), unitraveling-carrier photodiode (UTC-PD).

## I. INTRODUCTION

COHERENT fiber-optic links that utilize phase modulation can demonstrate high spur-free dynamic range and high signal-to-noise ratio. The challenge with phase modulation is building a coherent receiver that can linearly demodulate the phase of the received signal. To overcome this, we have demonstrated a novel coherent receiver architecture employing feedback for closely tracking the phase of the received signal [1], [2]. The incoming signal is mixed with a local oscillator signal and the detected photocurrent representing the phase difference is then fed back to a reference phase modulator. For high loop gain the signal phase is tracked closely. With a monolithically integrated approach, the delay of the feedback can be kept short enough for operation in the gigahertz (GHz) frequency range.

A very important requirement of this coherent receiver is the realization of photodiodes (PDs) that demonstrate both high output saturation current and high linearity at GHz frequencies and can be monolithically integrated with optical phase

modulators and couplers. The unitraveling-carrier photodiode (UTC-PD) is designed for high speed and high current operation [3]. We have previously demonstrated a monolithic balanced UTC-PD with a tunable multimode interference coupler on a platform that allows for the integration of MQW phase modulators [4]. In a UTC-PD light is absorbed in an undepleted p-type narrow bandgap layer, referred to as the absorber, and photo-generated electrons subsequently diffuse to a wide bandgap drift layer, referred to as the collector. Electrons are the only active carriers and electrons have a higher drift velocity than holes, therefore space charge saturation effects are reduced when compared to a p-i-n PD.

Several techniques for improving the performance of UTC-PDs have been demonstrated. Charge compensation was used to improve the saturation current by intentionally n-doping the collector layer [5]. By doing so, the electric field is preconditioned to be higher in the presence of a large mobile space charge density. Others have reported an enhancement in the response of UTC-PDs that have a graded doping profile in the p-type absorber [6]. This grade results in a potential profile that can aid electron transport. This same effect was also observed for UTC-PDs with uniform but relatively lower absorber doping [7].

We previously reported waveguide UTC-PDs that demonstrated output saturation currents greater than 40 mA at 1 GHz and a third-order output intercept point (OIP3) of 43 dBm at 20 mA and 34 dBm at 40 mA [8]. We observed a significant improvement in the saturation characteristics for devices that had a wider input waveguide. Here we have closely investigated the effects of the doping profile in several layers of the UTC-PD structure on the output response, saturation current, and third-order intermodulation distortion (IMD3). In particular, two different waveguide UTC-PDs were fabricated and characterized. The most significant differences in these devices are the doping profiles in the absorber and collector layers. The devices are referred to as PD A and PD B. In PD A, the p-doping in the absorber layer is not only higher, but also more uniform. The n-doping in the collector layer of PD A is  $7 \times 10^{15} \text{ cm}^{-3}$  whereas that for PD B is  $6 \times 10^{16} \text{ cm}^{-3}$ . For PD B an enhancement in the output response is observed at high current. This is believed to be due to the combination of the lower and more graded absorber doping profile as well as the higher collector doping level. The lower and more graded doping level in the absorber results in a small field induced at high current levels, and the higher collector doping level provides charge compensation. Both PDs exhibit saturation current levels that, to the best of our knowledge, are some of the highest reported for waveguide PDs

Manuscript received July 24, 2007; revised October 9, 2007. This work was supported by the Defense Advanced Research Projects Agency (DARPA) PHOR-FRONT program under United States Air Force Contract FA8750-05-C-0265.

The authors are with the Materials Department and the Electrical and Computer Engineering Department at the University of California, Santa Barbara, CA 93106 USA (e-mail: klamkin@engineering.ucsb.edu).

Digital Object Identifier 10.1109/JQE.2007.914768

TABLE I  
UTC-PD LAYER STRUCTURE

Layer	Thickness (nm)	Doping ( $\text{cm}^{-3}$ )
p-InGaAs contact	150	2E19
p-InP cladding	2,000	1E18
<b>p-InGaAs absorber</b>	<b>75</b>	<b>P</b>
InGaAs	8	UID
InGaAsP	16	UID
InP	6	UID
n-InP	7	1E18
<b>n-InP collector</b>	<b>200</b>	<b>N</b>
n-InP field termination	25	2E18
n-InGaAsP stop etch	15	5E17
n-InP	15	5E16
InGaAsP MQW and waveguide		
n-InP	600	1E18
n-InGaAsP contact	100	3E18
n-InP	500	1E18
SI InP substrate	350,000	

at comparable frequencies. For PD B, the OIP3 increases with photocurrent more so than for PD A. PD B exhibits higher linearity at high photocurrent levels.

## II. DEVICE DESIGN AND FABRICATION

The epitaxial structures are grown by metalorganic chemical vapor deposition (MOCVD) on semi-insulating InP substrates. The PD structures are grown directly above an InGaAsP optical waveguide. Passive regions are formed by selectively removing the PD layers using wet chemical etching. This step is followed by a blanket p-InP cladding and p-InGaAs contact layer regrowth. Surface ridges are formed, and metal contacts are deposited and annealed. Benzocyclobutene dielectric is used to reduce parasitic capacitance. The layer structure in a photodetection region following regrowth is shown in Table I. The p-doping level in the absorber and the n-doping level in the collector are denoted p and n, respectively. The doping levels for those layers, which are unintentionally doped are denoted UID. The n-InP field termination layer terminates the applied field across the collector layer of the PD in the photodetection regions and prevents depletion of the optical waveguide below. A cross section SEM image of a fabricated device is shown in Fig. 1. Light is coupled from a lensed fiber into the optical waveguide in a passive region and then absorbed as it propagates in a photodetection region. Because of the spatial separation of the absorber layer in the UTC-PD structure and the peak of the incoming optical mode, carrier generation is distributed more uniformly along the length of the device. This as well as a wide input waveguide help to reduce front-end saturation.

Of particular interest in understanding the device performance are the doping profiles in the absorber and collector layers. Zn is used for p-doping and Si is used for n-doping. The Zn and Si concentration in the structures were measured by secondary ion mass spectroscopy. The doping profiles are shown in Fig. 2. The absorber p-doping level was intended to be greater than  $2\text{E}18 \text{ cm}^{-3}$ . Because of the high diffusivity of Zn at growth temperatures, the grading in the doping profile can vary. For PD B, the peak Zn concentration in the absorber is 25% lower than that for PD A and the profile is more graded (high to low) toward the absorber/collector interface. These characteristics should result in a higher induced electric field in the absorber region of PD B and therefore a larger enhancement

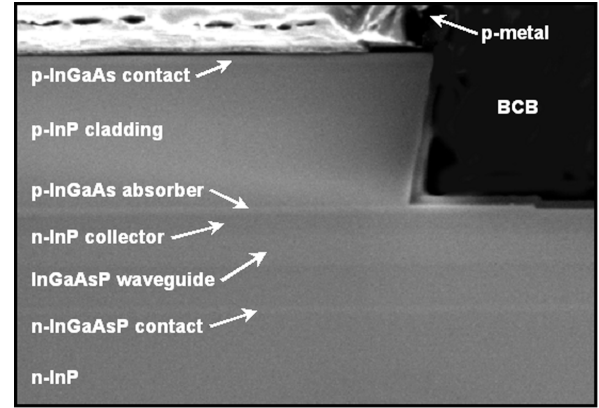


Fig. 1. Cross section SEM image of PD structure.

in the output response. The Si concentration in the collector of PD A is  $7\text{E}15 \text{ cm}^{-3}$  and that for PD B is  $6\text{E}16 \text{ cm}^{-3}$ , nearly an order of magnitude higher. The latter is adequate for providing charge compensation. Devices were fabricated with various geometries. The results that follow are for devices that are  $10 \mu\text{m}$  wide and  $150 \mu\text{m}$  long.

## III. RESULTS AND DISCUSSION

The electrical frequency responses of the UTC-PDs were measured at various biases for photocurrent levels up to around 70 mA. Fig. 3 shows the RF power as a function of dc photocurrent at 1 GHz for both devices. The data is normalized to 0 dB. For these measurements the modulation depth was 50%. The saturation characteristics of PD B vary with bias more so than those of PD A. The saturation current, defined here as the photocurrent level where the RF response is compressed by 1 dB, is around 65 mA for PD A and around 63 mA for PD B for a bias of  $-3.5 \text{ V}$ . Fig. 4 shows the RF power normalized to an ideal line with a slope of 20 dB/decade. For PD A, the response is fairly constant with increasing photocurrent until the onset of saturation. For PD B, there is a significant enhancement in the response with increasing photocurrent. This enhancement is due in part to a small field induced in the absorber at high photocurrent levels. The p-doping in the absorber of PD B is lower and more graded so this field should be greater in this device. The enhancement is also due to the higher n-doping in the collector of PD B. This doping provides some charge compensation and preconditions the electric field for operation at high photocurrent levels. Because the device areas are large, the 3-dB bandwidth is RC-limited. Therefore, any enhancement in the response should be attributed more so to improvements in the field distribution in the depletion region or the device capacitance rather than improvements in carrier transit time. For low biases the RF response of PD B saturates at much lower photocurrent levels than that of PD A. For example, at a bias of  $-2 \text{ V}$  the saturation current of PD B is less than 20 mA whereas for PD A it is greater than 40 mA. This is due to the fact that the doping in the collector layer of PD B is significantly higher. As such a higher bias is required to deplete the collector layer and optimize the field profile.

The internal quantum efficiency (IQE) was also measured for both PDs and the results are shown in Fig. 5. The PD structures

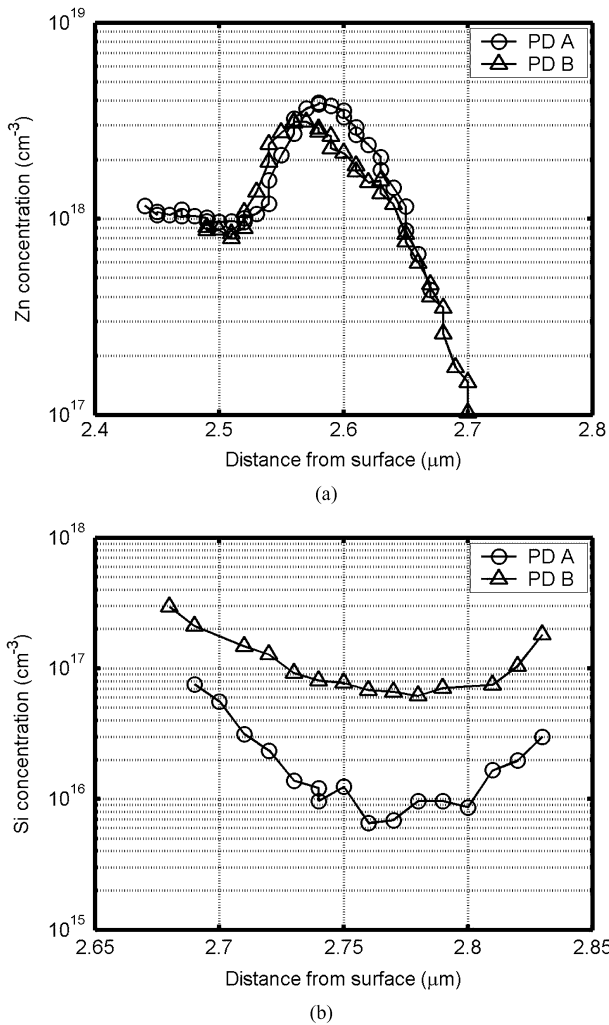


Fig. 2. (a) Zn doping profile in absorber and (b) Si doping profile in collector for both PDs.

are designed to be very efficient for the device length of 150  $\mu\text{m}$ . The IQE for PD A is around 99% and that for PD B is around 96%. For PD A the IQE is fairly constant with photocurrent and bias. For PD B there is a slight increase in IQE with increasing photocurrent. The IQE also degrades slightly at high photocurrent levels for low biases. The change in 3-dB bandwidth as a function of dc photocurrent level is shown in Fig. 6 for both PDs. As expected, there is a larger enhancement with increasing photocurrent for PD B. For this PD the 3-dB bandwidth is enhanced by as much as 40%–50% whereas for PD A it is enhanced by at most around 30%. The saturation current was also extracted at 0.5 and 2 GHz. For PD A, the saturation current at these frequencies is 67 and 62, mA respectively. For PD B it is 60 and 62 mA.

To characterize the linearity of the PDs, a two-tone setup was used similar to that in [9]. Tones were generated at 1 and 0.8 GHz. The output fundamental and IMD3 power were measured as a function of input modulation power at various photocurrent levels and biases. Fig. 7 shows the IMD3 measurements for both devices at a photocurrent level of 30 mA and a bias of  $-5$  V. The OIP3 at these conditions for PD A is 35.8 dBm and that for PD B is 37.2 dBm. The input modulation power

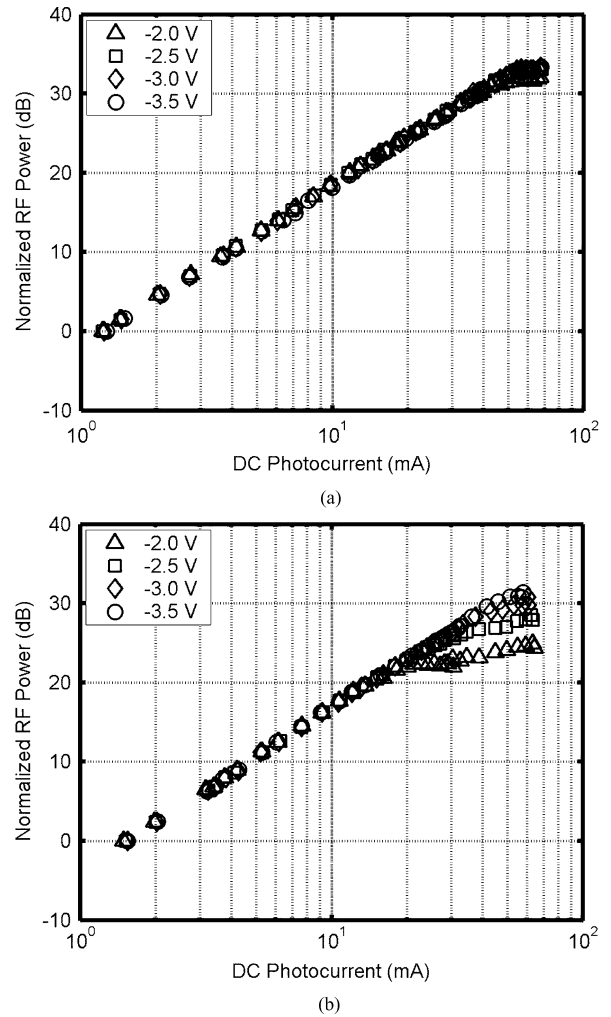
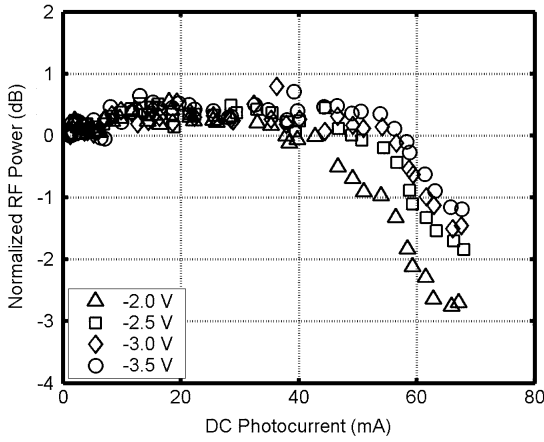
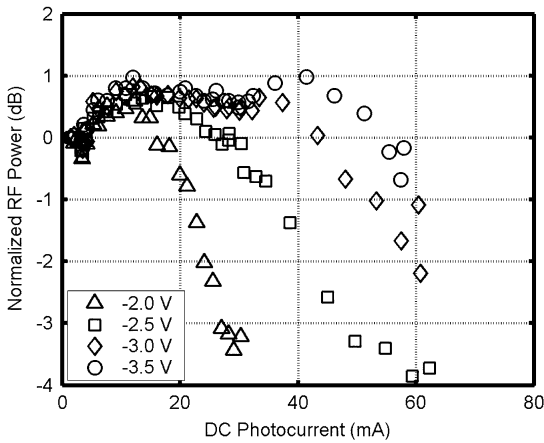


Fig. 3. Normalized RF power as a function of dc photocurrent at 1 GHz for (a) PD A and for (b) PD B.

levels applied correspond to a modulation index range of around 62%–82%. Fig. 8 shows the OIP3 as a function of dc photocurrent for both PDs. For these measurements the bias for both devices was  $-5$  V and the input RF tones were 1 and 0.8 GHz as before. At 10-mA dc photocurrent, PD A demonstrates a significantly higher OIP3. However at higher photocurrent levels, the OIP3 for PD B is higher. This is consistent with the saturation characteristics observed. The enhancement in OIP3 with increasing photocurrent is typical of UTC-PDs. The authors in [10] attribute this to the electric field induced in the absorber layer, which improves the RF response. For PD B the increase in OIP3 in going from 10 to 20 mA of photocurrent is greater than that for PD A. It is possible that because the absorber layer doping profile in PD B is lower and more graded, the induced electric field is greater and therefore the enhancement in the RF response and in turn the OIP3 is greater. This does not however explain why the OIP3 of PD B is lower at the lower photocurrent level. The n-doping level of PD B is  $6 \times 10^{16} \text{ cm}^{-3}$  and that for PD A is  $7 \times 10^{15} \text{ cm}^{-3}$ . The doping level in PD B is sufficient for providing charge compensation, which preconditions the electric field for high photocurrent levels. This also contributes to the enhancement in OIP3 at higher photocurrent levels. Because of the

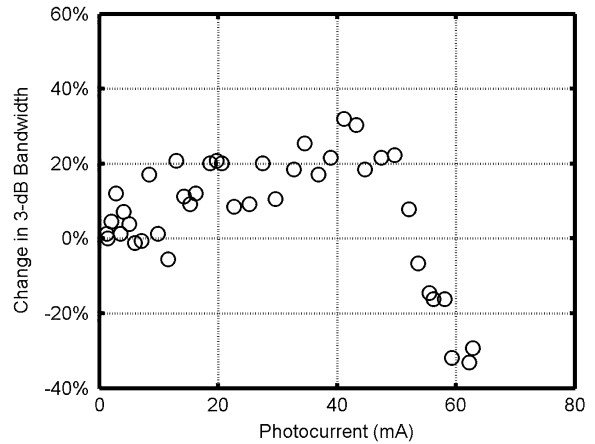


(a)

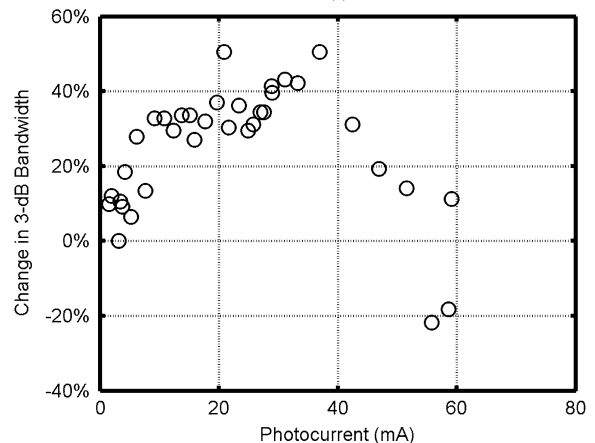


(b)

Fig. 4. Normalized RF power as a function of dc photocurrent at 1 GHz for (a) PD A and for (b) PD B.



(a)



(b)

Fig. 6. Change in 3-dB bandwidth as a function of dc photocurrent for (a) PD A and for (b) PD B. The bias is  $-3.5$  V for both devices.

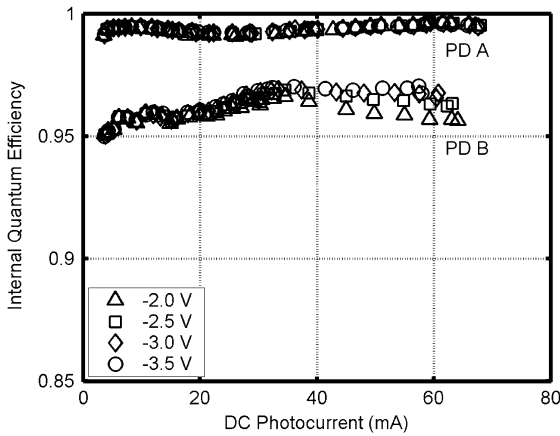


Fig. 5. Internal quantum efficiency as a function of dc photocurrent for PD A and PD B.

higher doping in PD B, at low photocurrent levels the collector layer may only be partially depleted and therefore the response is degraded when compared to PD A. In general increasing the bias reduces space charge saturation and enhances both the RF response and the OIP3 [4], [11]. For PD B a higher bias may therefore be required at low photocurrent levels in order to deplete the field layer and achieve higher OIP3.

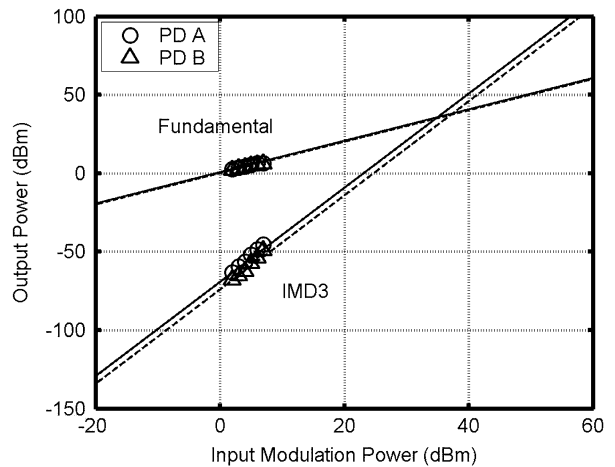


Fig. 7. IMD3 measurements at 30 mA for PD A and for PD B. The bias is  $-5$  V for both devices.

The OIP3 was also measured for other frequency tones at a fixed photocurrent level of around 40 mA. Fig. 9 shows the OIP3 as a function of the higher frequency tone ( $f_2$ ). For PD A, the OIP3 is fairly constant and begins to degrade slightly as  $f_2$  approaches 1.0 GHz. For PD B, the OIP3 degrades with  $f_2$

## IV. CONCLUSION

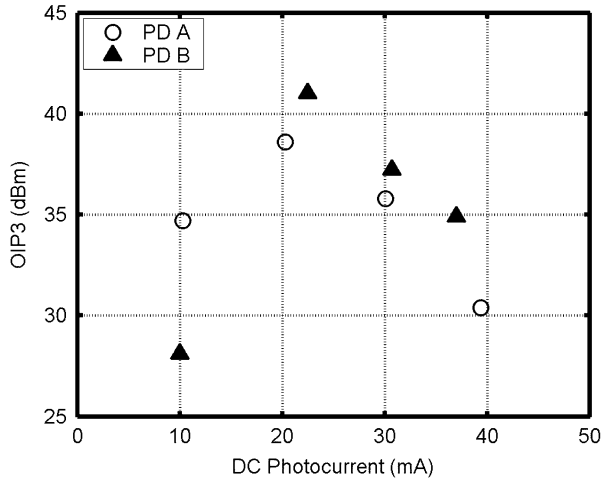


Fig. 8. OIP3 as a function of dc photocurrent for PD A and PD B. The bias is  $-5$  V for all measurements.

We have fabricated and tested UTC-PDs with different absorber and collector layer doping profiles. An enhancement in the response is observed for PD B, which has a lower and more graded absorber doping as well as a higher collector doping. These result in a higher induced field in the absorber layer and charge compensation respectively. Saturation currents of 65 mA for PD A and 63 mA for PD B are demonstrated. To the best of our knowledge these represent some of the highest saturation currents reported for waveguide PDs. IMD3 measurements were also performed to investigate the effects of the response enhancement of PD B on linearity. The OIP3 at a photocurrent level of 10 mA is 34.7 dBm for PD A and 28.1 dBm for PD B. However at higher photocurrent levels, the OIP3 for PD B is higher than that for PD A. At 40 mA for example, the OIP3 of PD B is 34.9 dBm whereas for PD A it is 30.4 dBm. PD B is therefore preferable for high current operation.

## REFERENCES

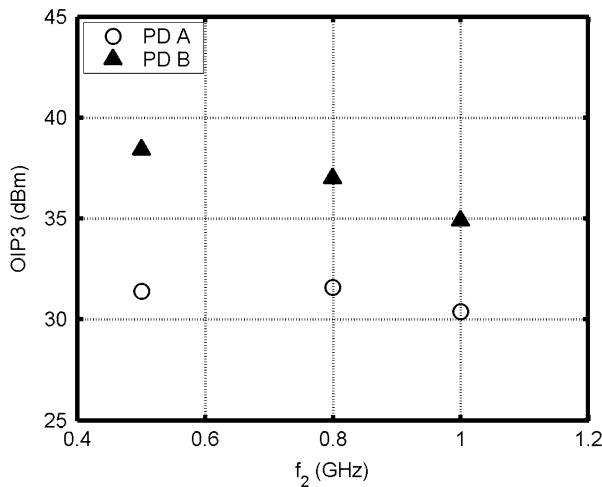


Fig. 9. OIP3 as a function of the higher frequency tone ( $f_2$ ) for PD A and PD B. The photocurrent level is 40 mA and the bias is  $-5$  V for all measurements.

however the OIP3 of PD B is higher than that of PD A at all of the measured values of  $f_2$ .

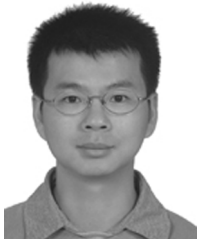
It appears that because of its enhanced response, PD B exhibits a higher OIP3 at high photocurrent levels. Overall PD B seems to perform better, however the design of the PD structure, namely the doping profiles in the absorber and collector layers, can be tailored for a specific region of operation. Recall that for the same bias, PD A exhibits a higher OIP3 at a photocurrent level of 10 mA. To reach the same OIP3 at this photocurrent level, PD B requires a higher bias. If heat dissipation is considered, PD A is favorable for operation at low photocurrent levels. However at all measured photocurrent levels above 10-mA PD B exhibits a higher OIP3 for the same bias, therefore PD B is favorable for high current operation.

- [1] H.-F. Chou, A. Ramaswamy, D. Zibar, L. A. Johansson, J. E. Bowers, M. Rodwell, and L. Coldren, "SFDR improvement of a coherent receiver using feedback," presented at the Coherent Optical Technol. Appl. Conf., 2006, Paper CFA3.
- [2] A. Ramaswamy, L. A. Johansson, J. Klamkin, C. Sheldon, H.-F. Chou, M. J. Rodwell, L. A. Coldren, and J. E. Bowers, "Coherent receiver based on a broadband optical phase-lock loop," presented at the OFC Postdeadline Papers, 2007, Paper PDP3.
- [3] T. Ishibashi, T. Furuta, H. Fushimi, S. Kodama, H. Ito, T. Nagatsuma, N. Shimizu, and Y. Miyamoto, "InP/InGaAs uni-traveling-carrier photodiodes," *IEICE Trans. Electron.*, vol. E83-C, no. 6, pp. 938–949, Jun. 2000.
- [4] J. Klamkin, A. Ramaswamy, H.-F. Chou, M. N. Sysak, J. W. Raring, N. Parthasarathy, S. P. DenBaars, J. E. Bowers, and L. A. Coldren, "Monolithically integrated balanced uni-traveling-carrier photodiode with tunable MMI coupler for microwave photonic circuits," in *Proc. Conf. Optoelectron. Microelectron. Materials Devices*, 2006, pp. 184–187.
- [5] N. Li, X. Li, S. Demiguel, X. Zheng, J. C. Campbell, D. A. Tulchinsky, K. J. Williams, T. D. Isshiki, G. S. Kinsey, and R. Sudharsanan, "High-saturation-current charge-compensated InGaAs-InP uni-traveling-carrier photodiode," *IEEE Photon. Technol. Lett.*, vol. 16, no. 3, pp. 864–866, Mar. 2004.
- [6] N. Shimizu, N. Watanabe, T. Furuta, and T. Ishibashi, "InP-InGaAs uni-traveling-carrier photodiode with improved 3-db bandwidth of over 150 GHz," *IEEE Photon. Technol. Lett.*, vol. 10, no. 3, pp. 412–414, Mar. 1998.
- [7] N. Shimizu, N. Watanabe, T. Furuta, and T. Ishibashi, "Improved response of uni-traveling-carrier photodiodes by carrier injection," *Jpn. J. Appl. Phys.*, vol. 37, pp. 1424–1426, 1998.
- [8] J. Klamkin, A. Ramaswamy, L. A. Johansson, H.-F. Chou, M. N. Sysak, J. W. Raring, N. Parthasarathy, S. P. DenBaars, J. E. Bowers, and L. A. Coldren, "High output saturation and high-linearity uni-traveling-carrier waveguide photodiodes," *IEEE Photon. Technol. Lett.*, vol. 19, no. 3, pp. 149–151, Feb. 2007.
- [9] H. Jiang, D. S. Shin, G. L. Li, T. A. Vang, D. C. Scott, and P. K. L. Yu, "The frequency behavior of the third-order-intercept point in a waveguide photodiode," *IEEE Photon. Technol. Lett.*, vol. 12, no. 5, pp. 540–542, May 2000.
- [10] T. Ohno, H. Fukano, Y. M. T. Ishibashi, T. Yoshimatsu, and Y. Doi, "Measurement of intermodulation distortion in a unidirectional carrier refracting-facet photodiode and a p-i-n refracting-facet photodiode," *IEEE Photon. Technol. Lett.*, vol. 14, no. 3, pp. 375–377, Mar. 2002.
- [11] K. J. Williams and R. D. Esman, "Design considerations for high-current photodetectors," *J. Lightw. Technol.*, vol. 17, no. 8, pp. 1443–1454, Aug. 1999.



**Jonathan Klamkin** (S'04) received the B.S. degree in electrical and computer engineering from Cornell University, Ithaca, NY, in 2002, and the M.S. degree in electrical and computer engineering from the University of California, Santa Barbara (UCSB) in 2004, where he is currently working toward the Ph.D. degree in materials.

His research interests include the design, epitaxial growth, fabrication, and characterization of widely-tunable semiconductor lasers, photodetectors, optical intensity and phase modulators, compact couplers, and semiconductor optical amplifiers for InP-based photonic integrated circuits. Currently his efforts are focused on novel coherent integrated receivers for highly linear microwave photonic links.



**Yu-Chia Chang** received the B.S. degree in electrical engineering and the M.S. degree in electrooptical engineering from National Taiwan University, Taipei, Taiwan, R.O.C., in 1997 and 1999, respectively. He is currently working toward the Ph.D. degree in electrical and computer engineering, University of California, Santa Barbara (UCSB).

He worked for BenQ Inc., Taiwan, R.O.C., in 1999–2001 and National Taiwan University in 2001–2002. His current research interests are the design, growth, and characterization of high-efficiency

high-speed vertical-cavity surface-emitting lasers for optical interconnect applications.



**Anand Ramaswamy** (S'06) received the B.S. degree in electrical engineering with a minor in physics from the University of Southern California, Los Angeles, 2005 and the M.S. degree in electrical engineering from the University of California, Santa Barbara, in 2007, respectively, where he is currently working towards the Ph.D. degree under Professor John E. Bowers.

His research interests lie in coherent communication systems and non-linear mechanisms in high power photodetectors.

**Leif. A Johansson** received the Ph.D. degree in engineering from University College London, U.K., in 2002.

He took up a postdoctoral position at the University of California at Santa Barbara in 2002. His current research interests include design and characterization of integrated photonic devices for analog and digital applications.



**John E. Bowers** (F'93) received the M.S. and Ph.D. degrees from Stanford University, Stanford, CA.

He is a Professor in the Department of Electrical Engineering, and in the Technology Management Program at the University of California, Santa Barbara. He is also CTO and cofounder of Calient Networks. His research interests are primarily concerned with silicon photonics, optoelectronic devices, optical switching and transparent optical networks. He is cofounder of the Center for Entrepreneurship and Engineering Management, and

founder of Terabit Technology. He worked for AT&T Bell Laboratories and Honeywell before joining UCSB. He has published eight book chapters, 400 journal papers, 600 conference papers and has received 49 patents.

Dr. Bowers is a Fellow of OSA and the American Physical Society, and a recipient of the IEEE LEOS William Streifer Award and the South Coast Business and Technology Entrepreneur of the Year Award. He was an elected member of the IEEE LEOS Board of Governors, a LEOS Distinguished Lecturer, and Vice President for Conferences for LEOS. He is a member of the National Academy of Engineering. He received the ACE Award for Most Promising Technology for the hybrid silicon laser in 2007.



**Steven P. DenBaars** (F'05) is a Professor of materials and electrical and computer engineering, and the Co-Director of the Solid State Lighting and Display Center, at the University of California, Santa Barbara.

His research areas are in MOCVD growth of wide-bandgap semiconductors (GaN-based) and their application to blue LEDs and laser and high-power electronic devices.

Dr. DenBaars is the recipient of the Mitsubishi Chemical Endowed Chair in Solid State Lighting and Display.



**Larry A. Coldren** (F'82) received the Ph.D. degree in electrical engineering from Stanford University, Stanford, CA, in 1972.

He is the Fred Kavli Professor of Optoelectronics and Sensors at the University of California, Santa Barbara. After 13 years in the research area at Bell Laboratories, he joined UC-Santa Barbara in 1984 where he now holds appointments in materials and electrical and computer engineering, and is Director of the Optoelectronics Technology Center. In 1990, he co-founded Optical Concepts, later acquired

as Gore Photonics, to develop novel VCSEL technology; and in 1998 he co-founded Agility Communications, recently acquired by JDSU, to develop widely-tunable integrated transmitters. He has authored or co-authored over 800 papers, five book chapters, one textbook, and has been issued 61 patents. He has presented dozens of invited and plenary talks at major conferences.

Prof. Coldren is a Fellow of OSA, and IEE, U.K., the recipient of the 2004 John Tyndall Award, and a member of the National Academy of Engineering.